This version of the SI published 21/02/2025 replaces the previous version published 09/10/2023. A typographical error in the caption of Fig. S4 is corrected.

Supplementary Information

Construction of an autocatalytic reaction cycle in neutral medium for synthesis of life-sustaining sugars

Hiro Tabata‡ [a], Genta Chikatani‡ [a], Hiroaki Nishijima [a], Takashi Harada [a], Rika Miyake [a], Souichiro Kato [a,b], Kensuke Igarashi [b], Yoshiharu Mukouyama [a,c], Soichi Shirai [d], Minoru Waki [d], Yoko Hase* [a,d] and Shuji Nakanishi* [a,e]

[a.] *Research Center for Solar Energy Chemistry, Graduate School of Engineering Science, Osaka University, Toyonaka, Osaka, 560-8531, Japan. E-mail: nakanishi.shuji.es@osaka-u.ac.jp.*

[b.] *Bioproduction Research Institute, National Institute of Advanced Industrial Science and Technology (AIST), 2-17-2-1, Tsukisamu higashi, Toyohira, Sapporo, 062-8517, Japan.*

[c.] *Division of Science, College of Science and Engineering, Tokyo Denki University, Hatoyama, Saitama 350-0394, Japan.*

[d.] *Toyota Central R&D Labs., Inc., 41-1 Yokomichi, Nagakute, Aichi, 480-1192, Japan. E-mail: y-hase@mosk.tytlabs.co.jp*

[e.] *Innovative Catalysis Science Division, Institute for Open and Transdisciplinary Research Initiatives (ICS-OTRI), Osaka University, Suita, Osaka, 565-0871 Japan.*

‡These authors contributed equally to this work.

Table of Contents

Experimental Section

Materials

All materials were used as purchased without further purification. 1,3-Dihydroxyacetone dimer, D-erythrose, D-(−)-ribose, D-(−)-lyxose, D-psicose, D-(+)-xylose, D-tagatose, D-(+)-talose, L-(−)-sorbose, D-(+)-allose, L-gulose, D-(+)-mannose, and D-(+)-galactose were purchased from Tokyo Chemical Industry. Glycolaldehyde dimer, DL-glyceraldehyde, L-(+)-erythrulose, D-ribulose, D-altrose and (2,4-dinitrophenyl)-hydrazine were obtained from Sigma-Aldrich Japan. Formaldehyde solution, D-(−)-arabinose, D-(+)-glucose, D-(−)-fructose, sodium hydroxide, methanol, acetonitrile, phosphoric acid, acetic acid, phenol, sulfuric acid, $Na_2WO_4 \bullet 2H_2O$ and $Na_2MoO_4 \bullet 2H_2O$ were purchased from FUJIFILM Wako. Phenylhydrazine was obtained from Kanto Chemical. Deionized and distilled water was supplied from a Millipore system.

Instruments

High-performance liquid chromatography (HPLC) analyses were performed with a Chromaster® system equipped with a UV/Vis detector (360 nm; 5430 diode array detector) using an InertSustain C18 column (150 mm, GL Sciences) and mixed solvent of water–acetonitrile (6:4, v/v) as the eluent at a flow rate of 1.0 mL min^{-1}. HPLC analyses for sugars were performed using a HPLC Chromaster® Sugar Analysis System (Hitachi) equipped with a fluorescence detector (5440 FL detector) and an NH2P-50 4E column (250 mm, Shodex) as the stationary phase. Solvent A (acetonitrile), solvent B (water), and solvent C (10% (v/v) phosphoric acid solution) were used as the mobile phases at a flow rate of 1.0 mL min^{-1}. The following gradient profile was applied: from 90% solvent A and 5% solvent B to 75% solvent A and 20% solvent B over 30 min, with constant 5% solvent C. An aqueous solution of acetic acid (44.3%), phosphoric acid (54.2%), and phenylhydrazine (1.5%) was also added to the flow at a rate of 0.4 mL min^{-1} for the post-column analyses. HPLC analyses of formic acid were performed using a system equipped with a UV/Vis detector (L-2455, Hitachi) and two DE-413 (Shodex) columns. The mobile phase was 10 mM H_3PO_4 aqueous solution at a flow rate of 1.0 mL min^{-1}.

Formose reaction

Oxometalate catalysts (Na_2WO_4, Na_2MoO_4) and substrates (HCHO, **C2a**) were dissolved in solvent (water or 10% (v/v) CH_3OH aqueous solution) to make a 4 mL solution. The solution was placed in a screw-top vial with a stir bar. To initiate the formose reaction, the solution in the vial was heated to 80 °C while stirring using an organic synthesis stirrer (HHE-19G-US IV, KPI). At specific time points, the reaction was stopped by cooling the vial in ice water. Na^+ and oxometalate anions were then removed using cation exchange resin, Amberlite IR120BHAG (Organo), and anion exchange resin, Amberlite IRA402BLCl (Organo), respectively.

Derivatization and preparation for analysis

Derivatization for HPLC analysis was performed as follows. The solution obtained after the reaction (2.5 µL) was diluted by the addition of water (748 µL). 375 µL of 2,4-dinitrophenylhydrazine (DNPH) in acetonitrile (1 mg mL^{-1}) and 22.5 µL of aqueous phosphoric acid (20% (v/v)) were dropped into each diluted sample. The mixed solutions were then stirred at room temperature for 60 min before HPLC analysis. Samples for HPLC analysis of sugars were prepared by the addition of water (250 µL) and acetonitrile (500 µL) to 250 µL of the reaction mixture. Samples for the quantification of formic acid were prepared by neutralizing the formose solution with hydrochloric acid instead of an ion-exchange resin.

Analysis of chromatographic data

Baseline correction of raw chromatographic data was conducted using the analytical programs Chromassist data station for HPLC and HPLC for sugars, respectively. Peaks were identified by comparison to chromatograms of commercially available reagents or by comparing retention times and experimental conditions.

Phenol-sulfuric acid method.

The method was used for the quantitative analysis of pentoses and hexoses.[1] First, 1.5 g of phenol was dissolved in 48.5 mL of ultrapure water to make a 3% (w/w) phenol solution. Next, 100 µL of the sample (10–100 µg mL^{-1}) and 200 µL of 3% phenol solution were added to a test tube and stirred, and then 750 µL of concentrated sulfuric acid was added, and the mixture was stirred and left for 20 min. The absorbance of the solution at 490 nm and at 480 nm was measured to estimate the concentration of hexose and pentose, respectively. Calibration curves for hexose and pentose were obtained using glucose and xylose as standards, respectively.

Cultivation of microbial cells and quantification of sugar consumption.

Soil microbes were collected from forest soil near the National Institute of Advanced Industrial Science and Technology, Hokkaido, Japan. Samples were added to an inorganic medium[2] containing filter-sterilized formose solution and incubated at 30 °C with agitation. The formose solution fed to the microbial cultures was prepared as follows: 1 M HCHO aqueous solution containing 10 mM **C2a** and 60 mM Na_2WO_4 in the presence of 10% (v/v) CH_3OH was maintained at 80 °C for 4 h. After the reaction, catalysts were removed from the solution using an anion exchange resin. Unreacted HCHO and CH_3OH were also removed by freeze-drying. The resultant solid powder was re-dissolved in distilled water. After several days of incubation, microbial growth was observed, and the cultures were transferred to fresh medium after 7 days of incubation to enrich for microbes that metabolized the synthesized sugars. Microbial growth was confirmed by measuring the optical density at 600 nm (OD_{600}). Microbial community analyses were performed as described previously.[3] After incubation, the samples were filtered to obtain supernatants for further analyses.

Computational Methods

Density functional theory (DFT)-based theoretical analyses

DFT calculations were performed using the Gaussian09 program[4] with the B3LYP functional[5-8]. The basis set used was 6-31++G (d, p)[9-13] for C, H, O, and Na, whereas the Lanl2DZ basis set with the effective core potential[14-16] was used for W and Mo. Vibrational analysis was also performed for the optimized structures at the same level of theory to confirm the presence or absence of a vibrational mode with an imaginary number frequency and to obtain the Gibbs free energies. Here, the enthalpies and free energies below 298.15 K and 1 atm were evaluated. Intrinsic reaction coordinate calculations[17,18] were performed for transition state structures to confirm the connection to the reactant and product. The integral equation formalism polarizable continuum model[19,20] was used to consider the solvent effect of water. Charge densities were obtained by natural bond orbital (NBO) analysis[21]. The initial structures of sugars were taken from a previous report.[22]

Supplementary Discussion

Identification of HPLC peaks A–D

Some of the sugars formed in the formose reaction, including branched sugars, are not commercially available (see Fig. S13 for the HPLC peaks of commercially available sugar samples). Therefore, we attempted to identify the HPLC peaks obtained through analysis of the intermediate products of the formose reaction as substrates. (Note that stereoisomerism is not considered here.)

When the formose reaction was performed with oxometalates as catalysts, the concentration of C4 ketose (**C4k**) was significantly higher in the later stage of the reaction (Fig. 3b). When the reaction was performed using 0.3 M **C4k** as a substrate, the distribution of products obtained was very similar to that obtained in the reaction using HCHO as a substrate (Fig. S21). These results suggested that the products obtained using oxometalates as catalysts are C5–C6 monosaccharides synthesized from **C4k** as the main substrate. To test this hypothesis, the following experiments were performed.

First, to determine the structure of compounds A and B, acetylated samples were analyzed using ^{1}H-NMR, ^{13}C-NMR, and ESI-MS. To an aqueous solution of HCHO (1.0 M) and **C4k** (1.0 M) was added Na_2WO_4 (60 mM). After stirring at 60 °C for 1.5 h, Na_2WO_4 was removed from the mixture in a manner similar to the protocol described in the Experimental section. The obtained mixture was analyzed by HPLC, which revealed that compounds A and B were the major products (Fig. 4c). The mixture was lyophilized, and the residue was dissolved in a mixed solution of acetic anhydride (1 mL) and pyridine (1 mL). After the solution was stirred at room temperature overnight, 1 N HCl was added, and then the mixture was extracted with $CHCl_3$ (3 × 20 mL). The organic phase was dried over Na_2CO_3, and the solvent was removed *in vacuo*. The crude product was purified by silica gel chromatography using hexane-ethyl acetate (1:2, v/v) to yield 2-(acetoxymethyl)-3-oxobutane-1,2,4-triyl triacetate (compound A) and 3-hydroxy-4-oxopentane-1,2,5-triyl triacetate (compound B).

Spectroscopic data for 2-(acetoxymethyl)-3-oxobutane-1,2,4-triyl triacetate. ^{1}H NMR (400 MHz, $CDCl_3$): δ = 5.05 (s, 2H; AcO-CH_2-CO-), 4.30 (d, *J* = 1.84 Hz, 4H; (AcO-CH_2-)$_2$C(OAc)-CO-), 2.18 (s, 3H, CH_3-CO-O-), 2.12 (s, 6H; CH_3-CO-O-), 2.05 ppm (s, 3H; CH_3-CO-O-); ^{13}C-NMR (100 MHz, $CDCl_3$): δ = 203.5 (C=O), 171.0 (CH_3-*C*O-O-), 170.1 (CH_3-*C*O-O-), 80.0 ((AcO-CH_2-)$_2$*C*(OAc)-CO-), 66.8 (AcO-*C*H_2-CO-), 65.9 ((AcO-*C*H_2-)$_2$C(OAc)-CO-), 20.8 (*C*H_3-CO-O-), 20.6 (*C*H_3-CO-O-), 20.3 ppm (*C*H_3-CO-O-). ESI-MS *m/z* calcd. for $C_{13}H_{18}NaO_9$ $[M + Na]^+$: 341.0843; found: 341.0850 (data are shown in Fig. S22).

Spectroscopic data for 3-hydroxy-4-oxopentane-1,2,5-triyl triacetate. ^{1}H NMR (400 MHz, $CDCl_3$): δ = 5.32-5.24 (m, 1H; AcO-CH_2-C*H*(OAc)-CH(OH)-), 5.24 (s, 2H; AcO-CH_2-CO-), 4.86 (d, *J* = 8.24 Hz, 1H, AcO-CH_2-CH(OAc)-C*H*(OH)-), 4.01 (dq, *J* = 11.9, 5.04 Hz, 2H; AcO-CH_2-CH(OAc)-CH(OH)-), 2.19 (s, 3H; CH_3-CO-O-), 2.17 (s, 3H; CH_3-CO-O-), 2.10 ppm (s, 3H; CH_3-CO-O-); ^{13}C-NMR (100 MHz, $CDCl_3$): δ = 199.0 (C=O), 170.3 (CH_3-*C*O-O-), 170.0 (CH_3-*C*O-O-), 169.8 (CH_3-*C*O-O-), 88.7 (AcO-CH_2-*C*H(OAc)-CH(OH)-), 75.6 (AcO-CH_2-CH(OAc)-*C*H(OH)-), 68.6 (AcO-*C*H_2-CO-), 66.8 (AcO-*C*H_2-CH(OAc)-*C*H(OH)-), 20.8 (*C*H_3-CO-O-), 20.5 (*C*H_3-CO-O-), 20.3 ppm (*C*H_3-CO-O-). ESI-MS *m/z* calcd. for $C_{11}H_{16}NaO_8$ $[M + Na]^+$: 299.0737; found: 299.0749 (data are shown in Fig. S23).

Similarly, acetylated samples of compounds C and D were prepared in the same manner using **C2a** (1.0 M) and **C4k** (1.0 M) as substrates. HPLC analysis of the obtained mixture indicated that compounds C and D were the major products (Fig. 4d), whereas one acetylated compound (3-hydroxy-4-oxohexane-1,2,5,6-tetrayl tetraacetate) was obtained after purification.

Spectroscopic data for 3-hydroxy-4-oxohexane-1,2,5,6-tetrayl tetraacetate. ^{1}H NMR (400 MHz, $CDCl_3$): δ = 5.45 (dd, *J* = 5.49, 6.87 Hz, 1H; AcO-CH_2-C*H*(CH_2OAc)-CO-), 5.07 (d, *J* = 5.49 Hz, 2H; AcO-CH_2-C*H*(OAc)-CH(OH)-CO-), 4.34-4.23 (m, 2H; AcO-CH_2-CH(CH_2OAc)-CO-), 4.24-4.11 (m, 2H; AcO-CH_2-CH(OAc)-CH(OH)-CO-), 2.18 (s, 3H; CH_3-CO-O-), 2.14 (s, 3H; CH_3-CO-O-), 2.11 (s, 3H; CH_3-CO-O-), 2.02 ppm (s, 3H);

^{13}C NMR (100 MHz, $CDCl_3$): δ = 202.8 (C=O), 170.2 (CH_3-*C*O-O-), 170.0 (CH_3-*C*O-O-), 169.94 (CH_3-*C*O-O-), 169.87 (CH_3-*C*O-O-), 81.1 (AcO-CH_2-*C*H(CH_2OAc)-CO-), 71.7 (AcO-CH_2-*C*H(OAc)-CH(OH)-CO-), 66.9 (AcO-CH_2-CH(OAc)-*C*H(OH)-CO-), 66.2 (AcO-*C*H_2-CH(OAc)-CH(OH)-CO-), 61.0 (AcO-*C*H_2-CH(CH_2OAc)-CO-), 20.8 (*C*H_3-CO-O-), 20.5 (*C*H_3-CO-O-), 20.3 ppm (*C*H_3-CO-O-). ESI-MS *m/z* calcd. for $C_{14}H_{20}NaO_{10}$ $[M + Na]^+$: 371.0949; found: 371.0958 (data are shown in Fig. S24).

From these data, the species that gave the HPLC peaks were identified as 1,3,4-trihydroxy-3-(hydroxymethyl)butan-2-one (peak A), 1,3,4,5-tetrahydroxypentan-2-one (C5 ketose, **C5k**; peak B), and stereoisomers of 1,2,4,5,6-pentahydroxyhexan-3-one (3-hexulose, peaks C and D).

Reason for the suppression of the crossed Cannizzaro reaction under neutral conditions

The calculated free energy changes of deprotonation from **C2a**, **C4a**, and hydrated HCHO by WO_4^{2-} were 13.5, 8.5, and 12.8 kcal mol^{-1}, respectively, indicating that deprotonation from hydrated HCHO can occur thermodynamically. However, the activation energy for deprotonation depends on the relative configuration of the substrate and base in the respective transition state; the calculated structures of transition states are shown in Fig. S2, Fig. S10, and Fig. S18. The high activation energy shown in Fig. 5c has the potential to kinetically inhibit the Cannizzaro reaction for hydrated HCHO initiated by deprotonation.

Meanwhile, the preference of deprotonation is explained by the interaction between the HOMOs of the bases and the anti-bonding orbital σ* of the substrate (acid), H-A, to be deprotonated. The strength of the interaction between the HOMO of the base and the σ* of the acid is stronger when the energy difference between these orbitals is small; from DFT calculations, the energy of HOMO of the base, WO_4^{2-}, is determined to be −6.350 eV. The energy for σ* of α-hydrogen in **C2a** (substrate of aldol reaction, Fig. 2c), β-OH in **C4a** (substrate of retro-aldol reaction, Fig. 3d), and hydrated HCHO (HO-CH_2-OH, Fig. 5c) were estimated as −1.429, −0.325, and −0.236 eV, respectively. These results indicate that the interaction between WO_4^{2-} and hydrated HCHO is weaker than the interaction with **C2a** and **C4a**. Therefore, the deprotonation from hydrated HCHO did not proceed and the crossed Cannizzaro reaction was suppressed. Meanwhile, the energy of HOMO for OH^- was −5.491 eV that was higher than that of WO_4^{2-}, suggesting that deprotonation from hydrated HCHO was enabled to proceed (Fig. 5d).

Supplementary Figures and Tables

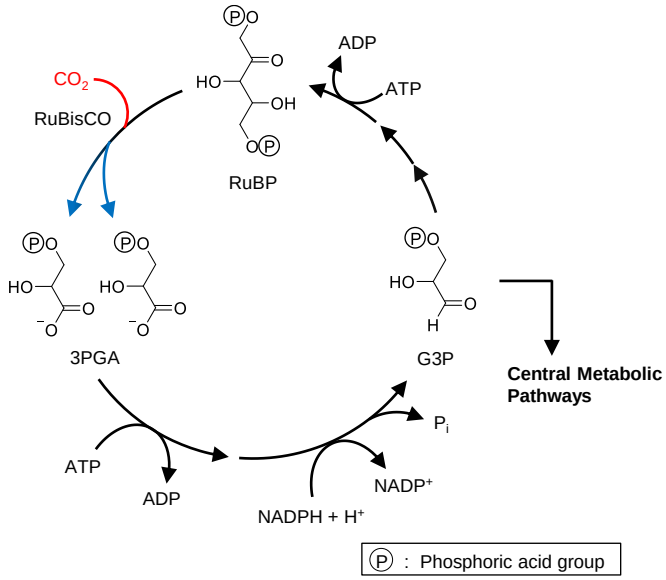

Fig. S1 Schematic diagram of the Calvin cycle.

Step	Structures
$A1_N$	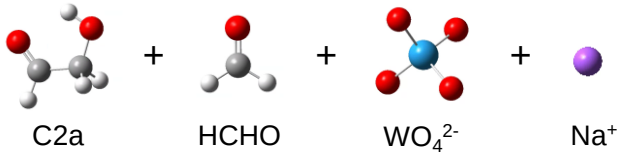 C2a + HCHO + WO_4^{2-} + Na^+
$TS1_N$	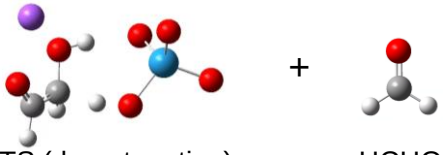 TS (deprotonation) + HCHO
$A2_N$	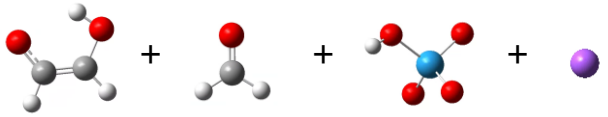 C2a enolate + HCHO + HWO_4^- + Na^+
$A3_N$	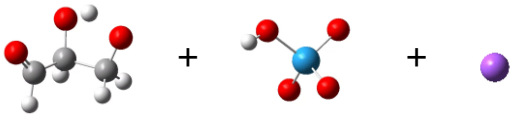 After C-C formation + HWO_4^- + Na^+
$A4_N$	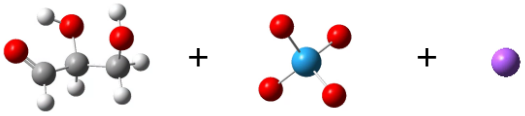 C3a + WO_4^{2-} + Na^+

Fig. S2 Optimized structures corresponding to the aldol reaction of **C2a** with HCHO, catalyzed by Na^+ and WO_4^{2-}. $A1_N$, $TS1_N$, $A2_N$, $A3_N$, and $A4_N$ correspond to Fig. 2d.

Step	Structures
$A1_B$	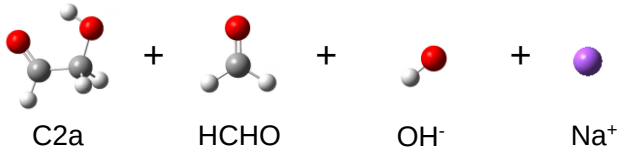 C2a + HCHO + OH^- + Na^+
$TS1_B$	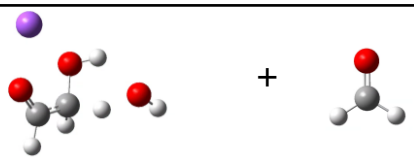 TS (deprotonation) + HCHO
$A2_B$	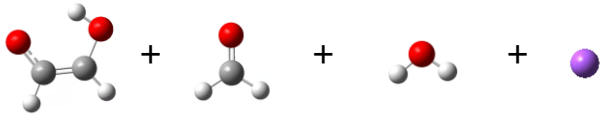 C2a enolate + HCHO + H_2O + Na^+
$A3_B$	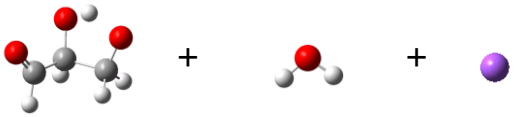 After C-C formation + H_2O + Na^+
$A4_B$	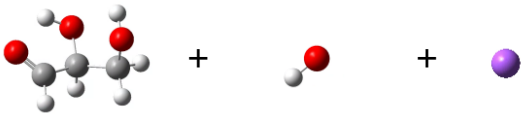 C3a + OH^- + Na^+

Fig. S3 Optimized structures corresponding to the aldol reaction of **C2a** with HCHO, catalyzed by Na^+ and OH^-. $A1_B$, $TS1_B$, $A2_B$, $A3_B$, and $A4_B$ correspond to Fig. 2d.

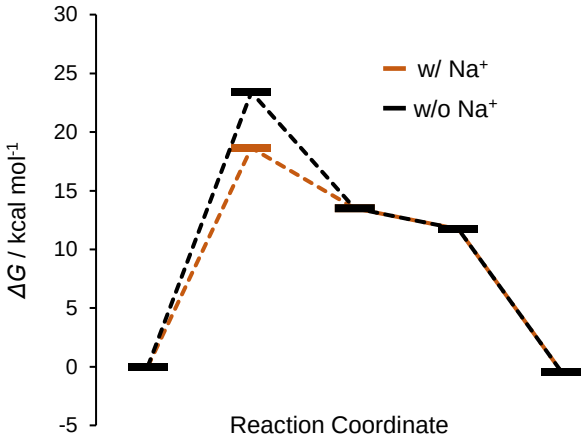

Fig. S4 Calculated free-energy diagram for the aldol reaction of **C2a** with HCHO catalyzed by WO_4^{2-} with Na^+ (brown) and without Na^+ (black) in water.

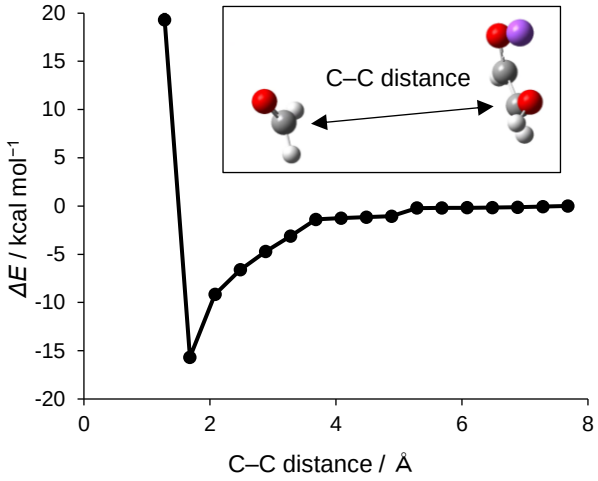

Fig. S5 Calculated C–C bond distance dependence of relative energy for C–C bond formation following α-H elimination.

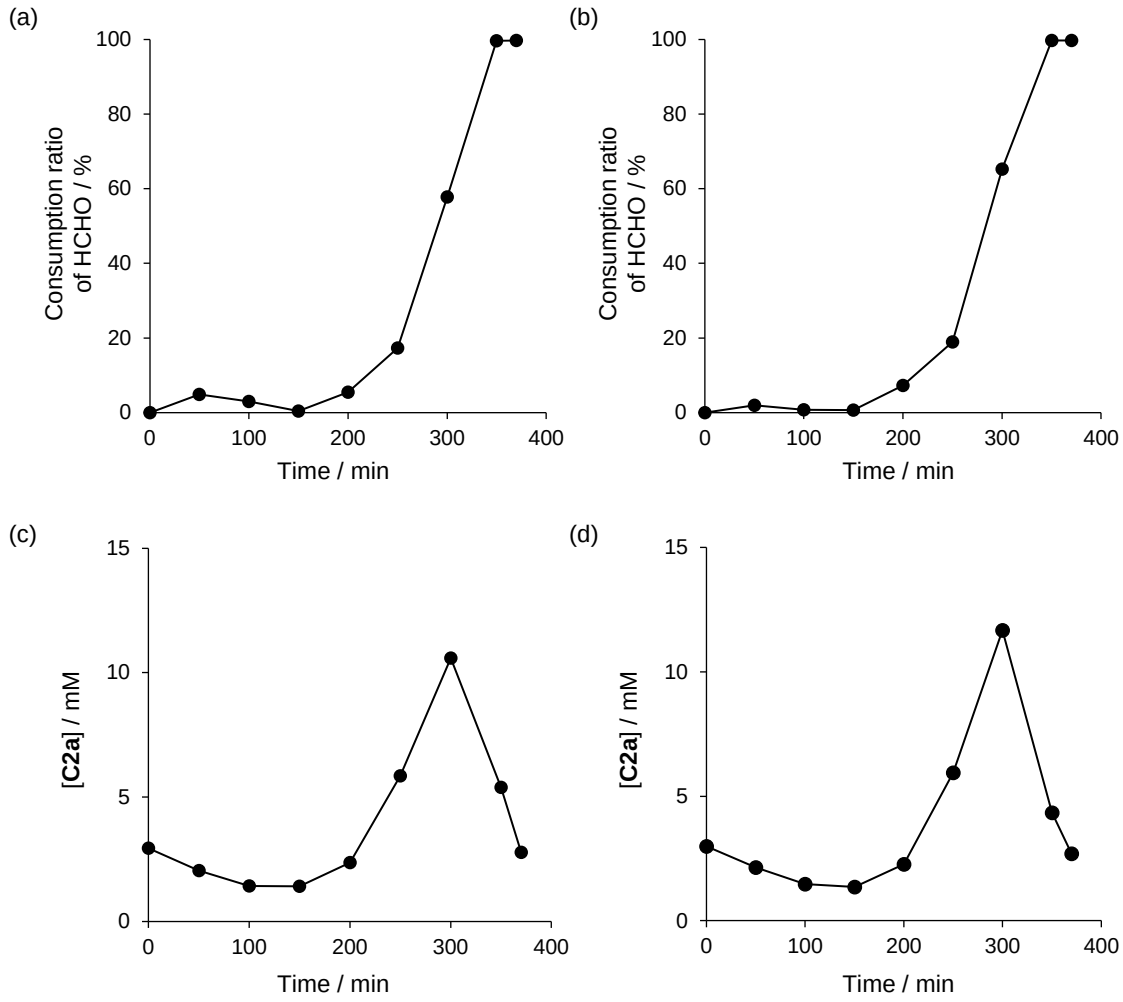

Fig. S6 Time course analysis of the consumption ratio of HCHO ((a), (b)) and **C2a** concentration ((c), (d)) for a solution containing initiator (**C2a**), catalyst (Na_2WO_4), and substrate (HCHO) heated at 80 °C. Although the induction period differed, similar trends to Fig. 3a and 3b were observed, with a sigmoidal consumption curve of HCHO and reproduction above the initial concentration of **C2a**.

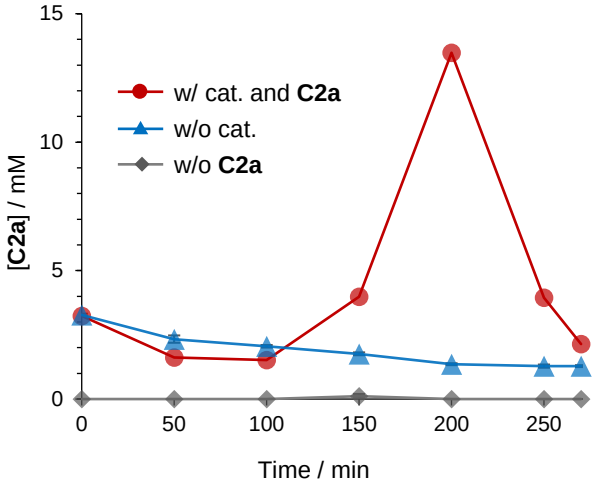

Fig. S7 Time course analysis of the **C2a** concentration under the same conditions. The gray and blue lines indicate the average of three experiments, respectively, and the error bars indicate standard errors. The red line was not assigned error bars due to variations in the induction period resulting from autocatalysis, although a similar trend was confirmed for at least three experiments (see Fig. S6).

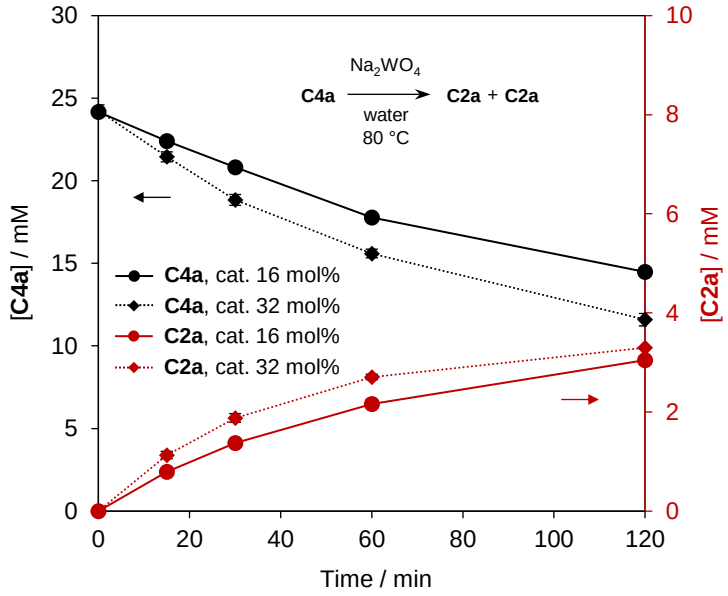

Fig. S8 Time course analysis of **C4a** (black) and **C2a** (red) concentrations when **C4a** containing Na_2WO_4 was heated at 80 °C. Results for catalyst concentrations of 16 and 32 mol% **C4a** are shown as dotted and solid lines, respectively. Three experiments were performed, and error bars indicate standard errors.

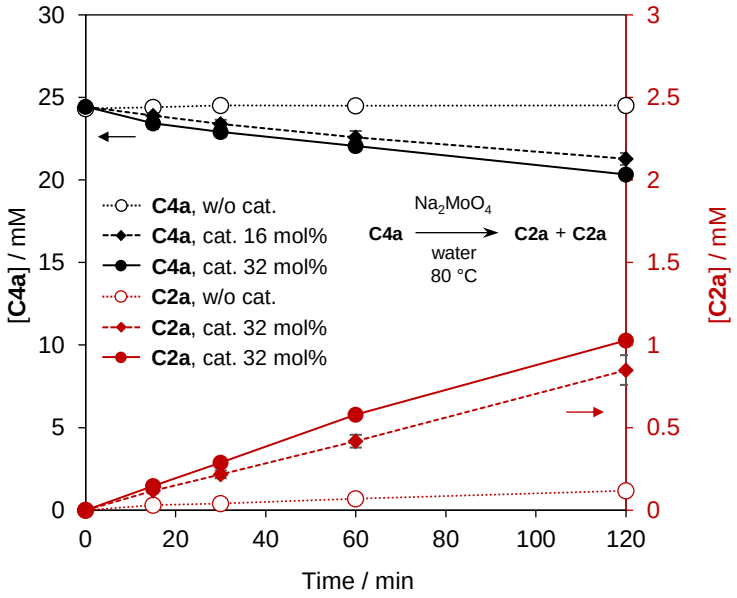

Fig. S9 Time course analyses of **C4a** (black) and **C2a** (red) concentrations when **C4a** containing Na_2MoO_4 was heated to 80 °C in water. The results obtained when no catalyst was added are shown as dotted lines with circles. The results obtained at a catalyst concentration of 16 mol% of **C4a** are shown as dotted lines with rhombi. The results obtained at a catalyst concentration of 32 mol% of **C4a** are shown as solid lines with circles. Three experiments were performed, and error bars indicate standard errors.

Step	Structures
$R1_N$	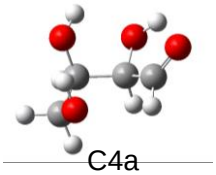 C4a +  WO_4^{2-} +  Na^+
$R2_N$	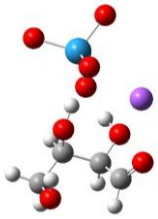 Before C-C cleavage
$TS2_N$	 TS (C-C cleavage)
$R3_N$	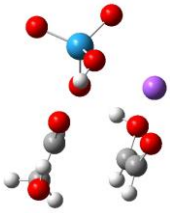 After C-C cleavage
$R4_N$	**2** 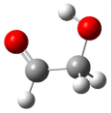 +  WO_4^{2-} +  Na^+ C2a

Fig. S10 Optimized structures for the retro-aldol reaction of **C4a** catalyzed by Na^+ and WO_4^{2-}. $R1_N$, $TS2_N$, $R2_N$, $R3_N$, and $R4_N$ correspond to Fig. 3d and 3e.

Step	Structures
$R1_B$	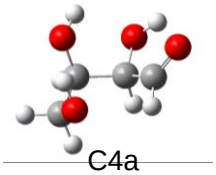 C4a +  OH^- +  Na^+
$R2_B$	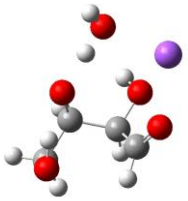 Before C-C cleavage
$TS2_B$	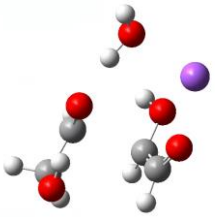 TS (C-C cleavage)
$R3_B$	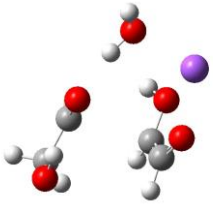 After C-C cleavage
$R4_B$	**2** 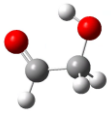 +  +  C2a OH^- Na^+

Fig. S11 Optimized structures for the retro-aldol reaction of **C4a** catalyzed by Na^+ and OH^-. $R1_B$, $TS2_B$, $R2_B$, $R3_B$, and $R4_B$ correspond to Fig. 3d and 3e.

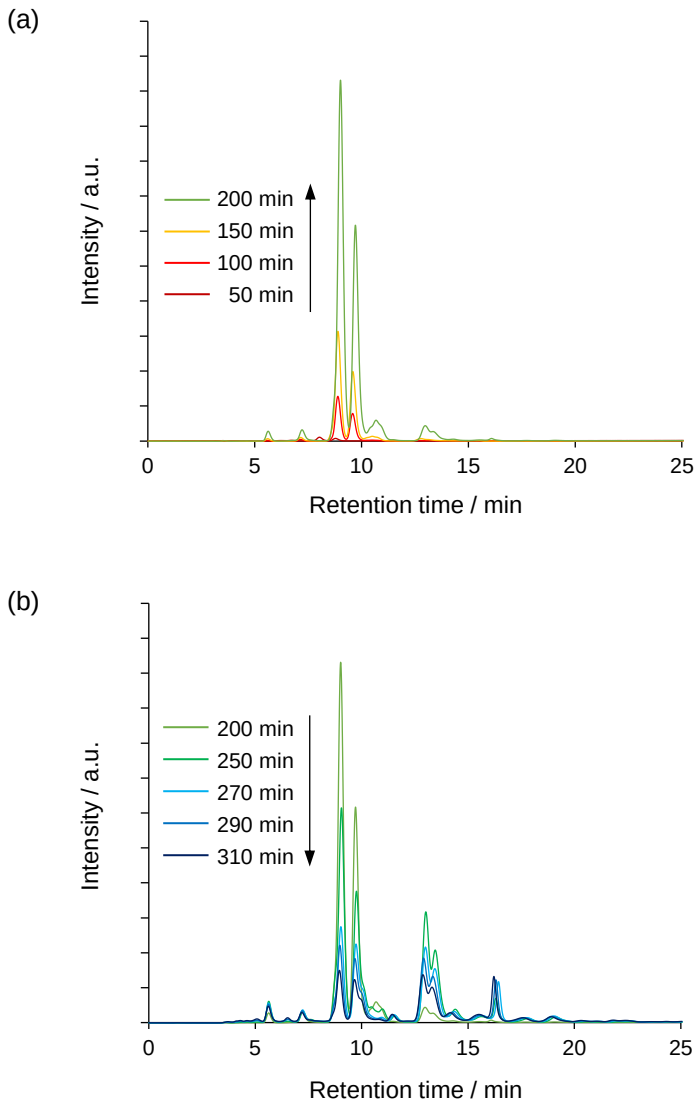

Fig. S12 (a) Time variation in sugar analysis HPLC chromatograms for 50–200 min. (b) Time variation of sugar analysis HPLC chromatograms for 200–310 min. These samples were obtained in the formose reaction in which HCHO (0.3 M) and **C2a** (3 mM) were heated at 80 °C in the presence of Na_2WO_4 catalyst (60 mM). The initial pH value was 7.82.

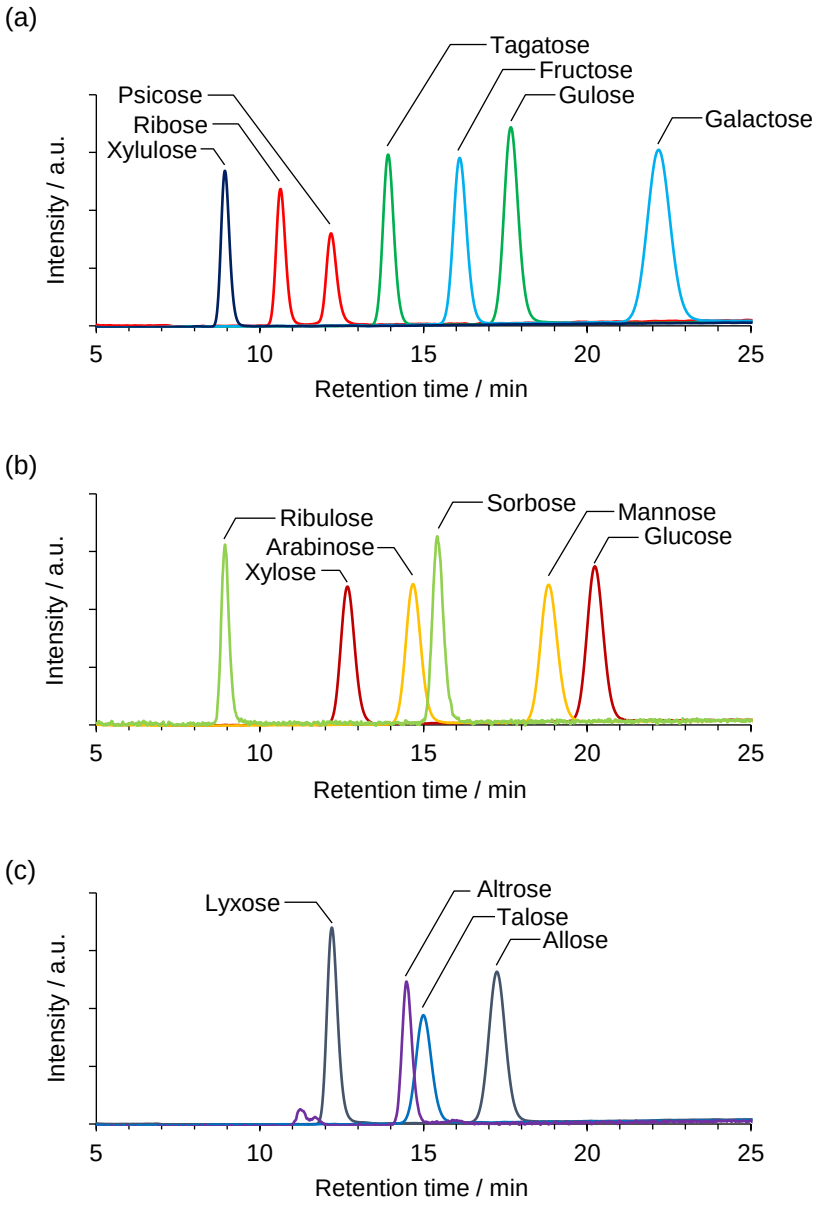

Fig. S13 HPLC chromatograms of commercially available monosaccharides. Xylulose, Ribose, Psicose and Talose were prepared as 0.625 mM aqueous solutions. Tagatose, Fructose, Gulose, Galactose, Ribulose, Xylose, Arabinose, Sorbose, Mannose, Glucose, Lyxose, Altrose and Allose were prepared as 1.25 mM aqueous solutions.

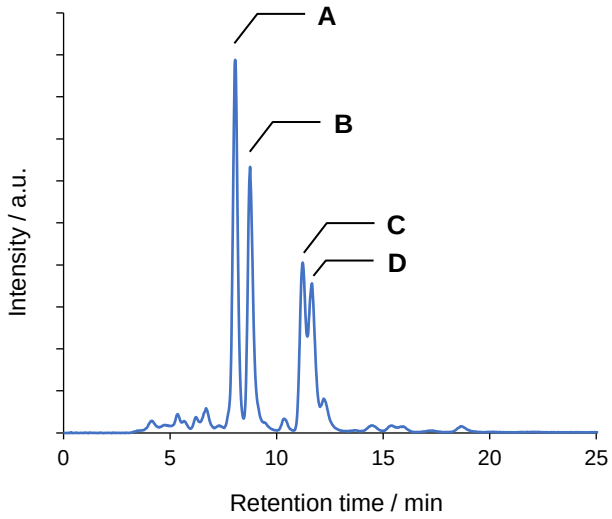

Fig. S14 Sugar analysis HPLC chromatogram of the formose reaction using 60 mM Na_2MoO_4 as a catalyst at 80 °C for 20 h. 0.3 M HCHO and 3 mM **C2a** were used as substrates of the formose reaction. The initial pH value was 7.42.

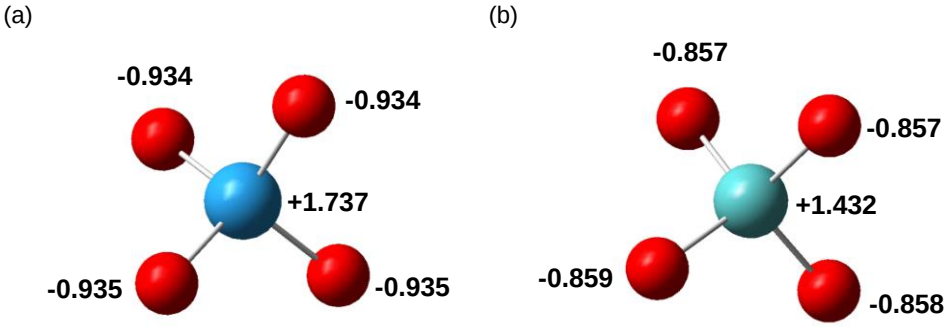

Fig. S15 Optimized structures and NBO charges of atoms in (a) WO_4^{2-} and (b) MoO_4^{2-}.

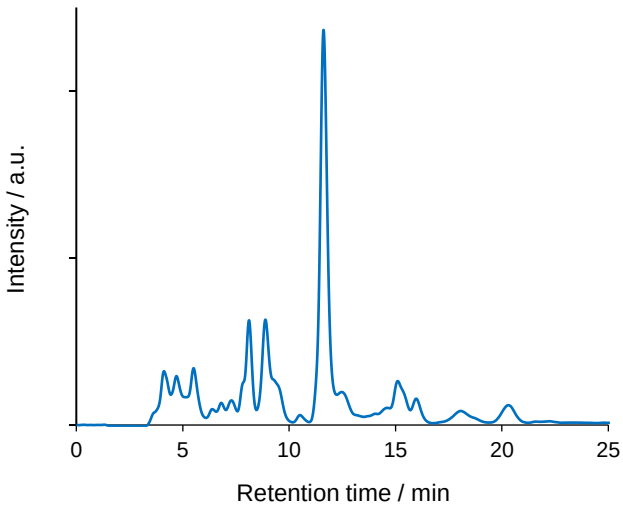

Fig. S16 HPLC chromatogram of the formose reaction using 60 mM NaOH as a catalyst at 80 °C for 17 min. 0.3 M HCHO and 3 mM **C2a** were used as substrates of the formose reaction. The initial pH value was 13.28.

Step	Structures
$C1_B$	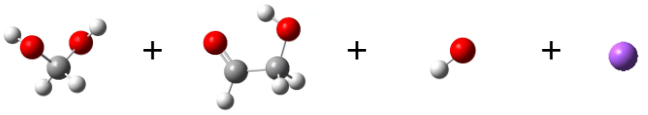 HCHO hydrate + C2a + OH^- + Na^+
$TS3_B$	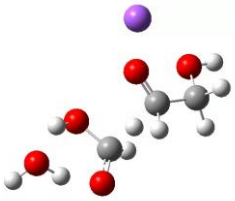 TS (H^- transfer)
$C2_B$	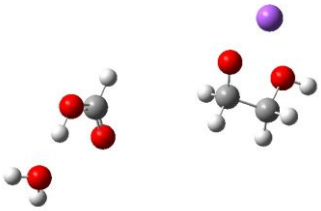 After H^- transfer
$C3_B$	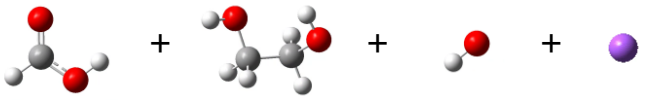 Formic acid + Ethylene glycol + OH^- + Na^+

Fig. S17 Optimized structures corresponding to the crossed Cannizzaro reaction of **C2a** with HCHO catalyzed by Na^+ and OH^-. $C1_B$, $TS3_B$, $C2_B$, and $C3_B$ correspond to Fig. 5d.

Step	Structures
$C1_N$	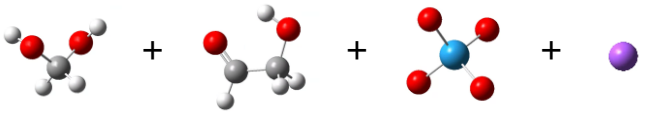 HCHO hydrate + C2a + WO_4^{2-} + Na^+
$TS3_N$	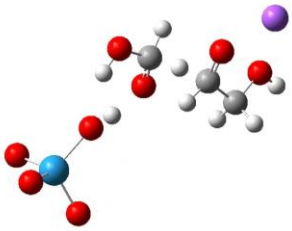 TS (H^- transfer)
$C2_N$	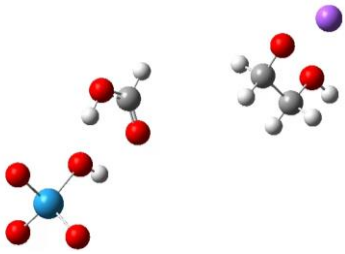 After H^- transfer
$C3_N$	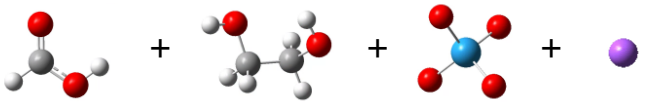 Formic acid + Ethylene glycol + WO_4^{2-} + Na^+

Fig. S18 Optimized structures corresponding to the crossed Cannizzaro reaction of **C2a** with HCHO catalyzed by Na^+ and WO_4^{2-}. $C1_N$, $TS3_N$, $C2_N$, and $C3_N$ correspond to Fig. 5d.

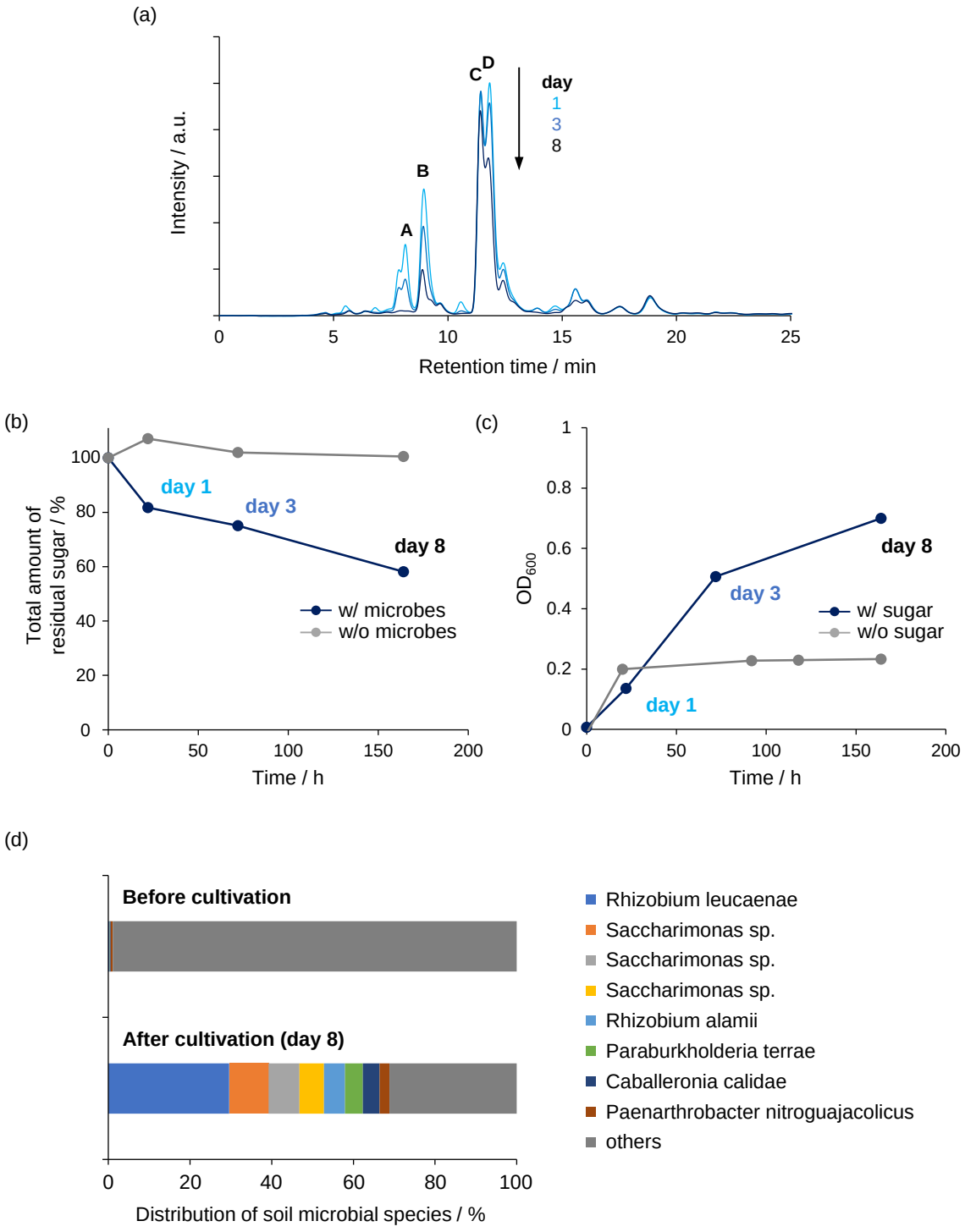

Fig. S19 Results of each of the experiments in Fig. 6 with different flora.

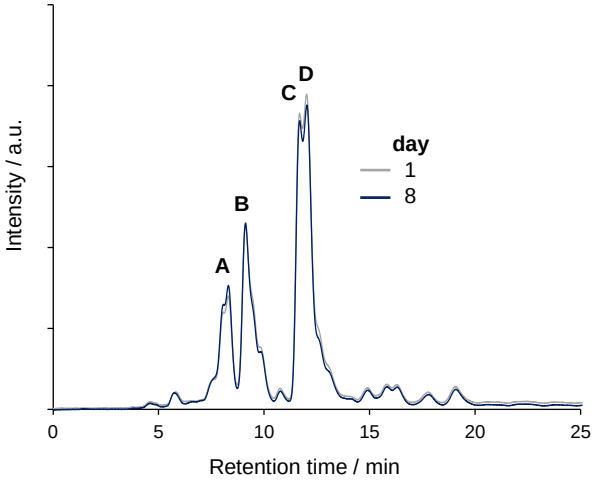

Fig. S20 HPLC chromatograms of the inorganic medium with the synthesized sugar at 1 and 8 days after the solution was prepared.

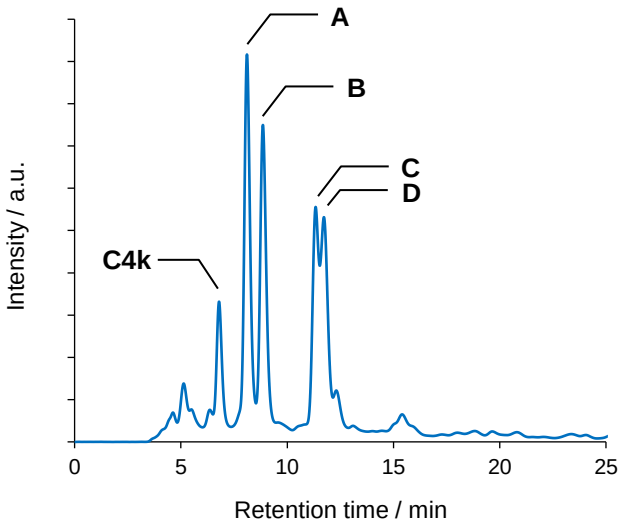

Fig. S21 Sugar analysis chromatogram of a solution of 10% aqueous methanol containing 300 mM **C4k** and 60 mM Na_2WO_4 heated at 80 °C for 60 min.

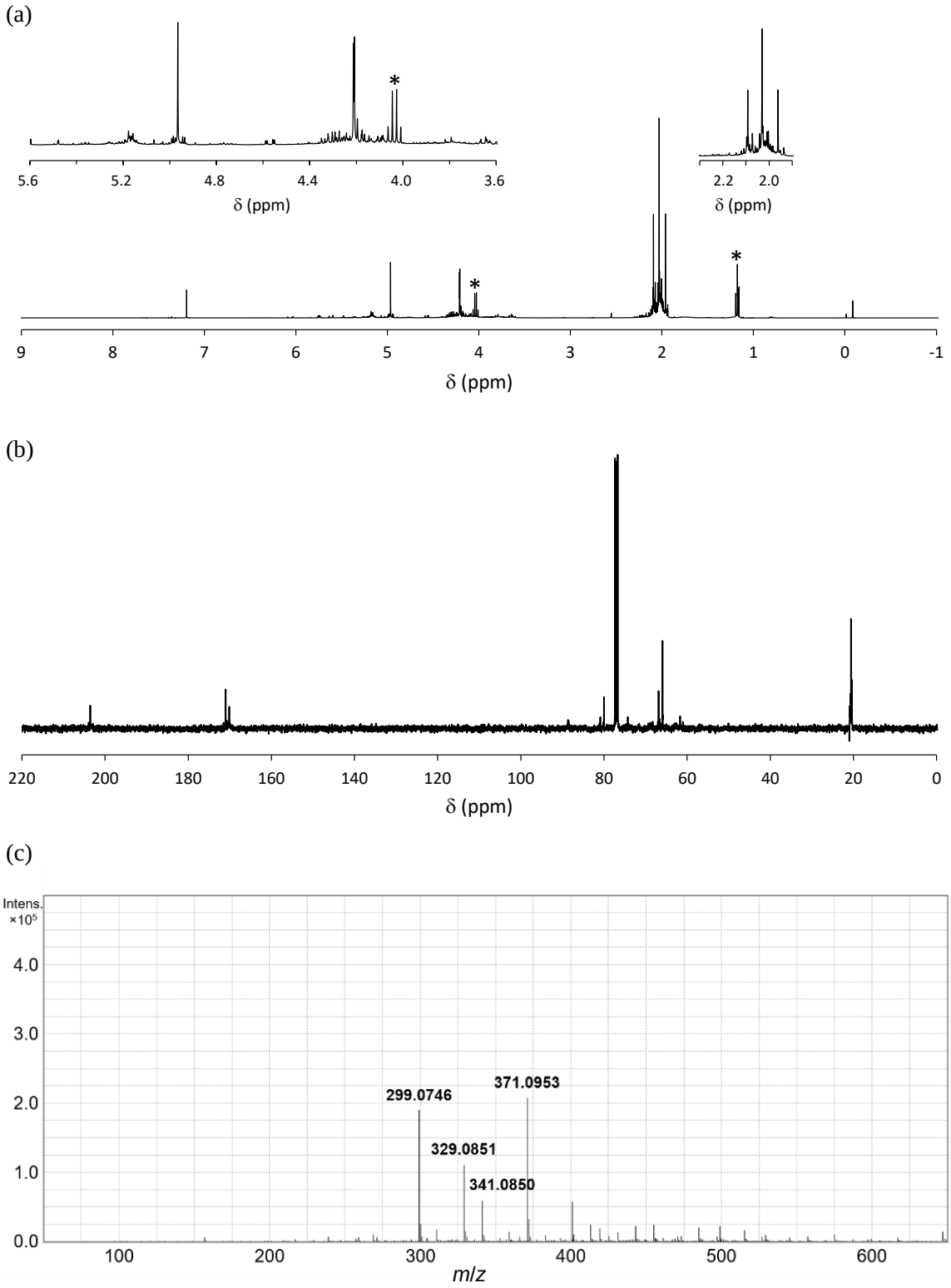

Fig. S22 ^{1}H-NMR, ^{13}C-NMR, and ESI-MS spectra of 2-(acetoxymethyl)-3-oxobutane-1,2,4-triyl triacetate. (a) ^{1}H-NMR spectrum. The peaks of ethyl acetate residues are marked with an asterisk. (Insets) Expanded images of spectrum. (b) ^{13}C-NMR spectrum. (c) ESI-MS spectrum.

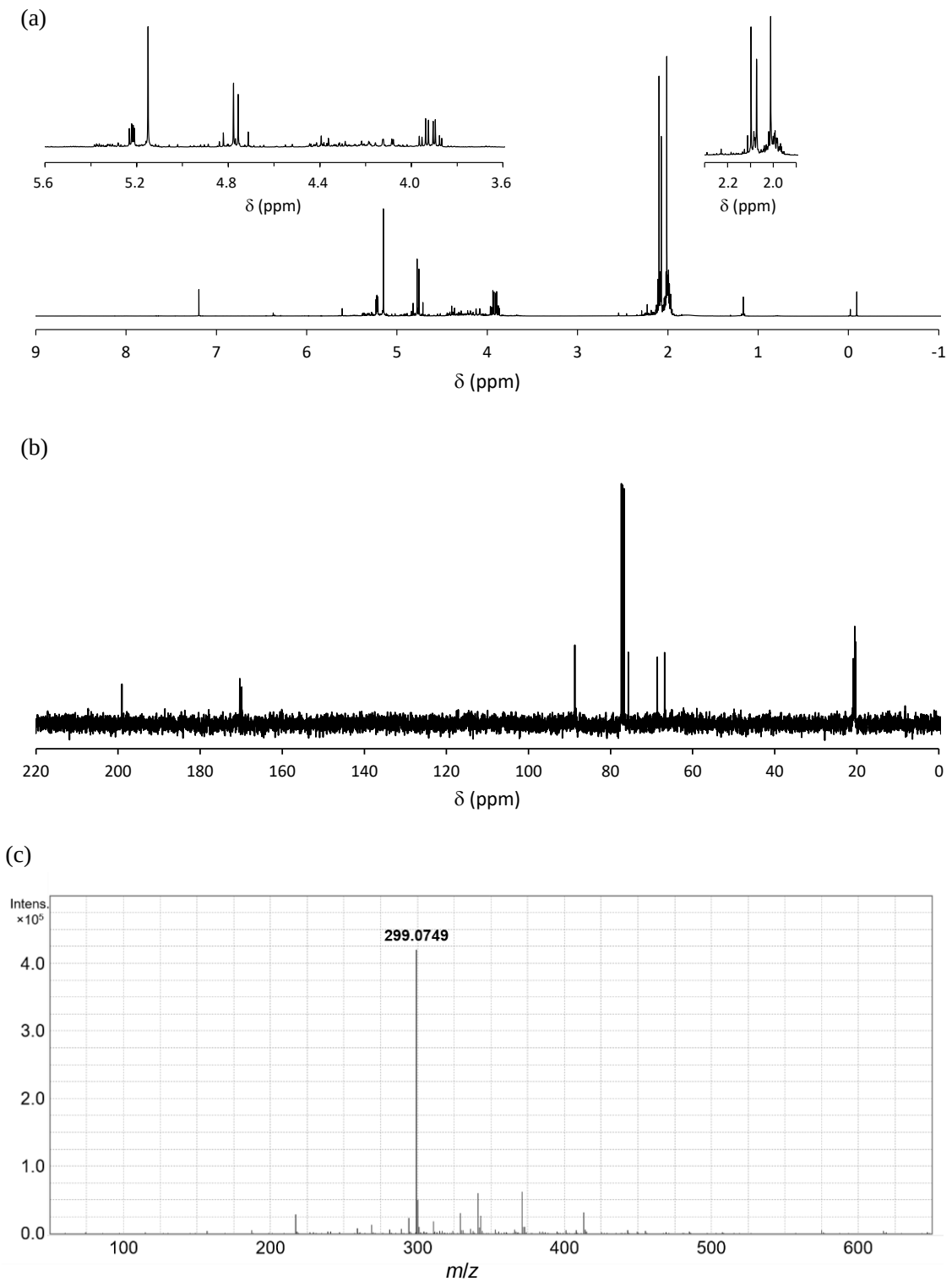

Fig. S23 ^{1}H-NMR, ^{13}C-NMR, and ESI-MS spectra of 3-hydroxy-4-oxopentane-1,2,5-triyl triacetate. (a) ^{1}H-NMR spectrum. (Insets) Expanded images of spectrum. (b) ^{13}C-NMR spectrum. (c) ESI-MS spectrum.

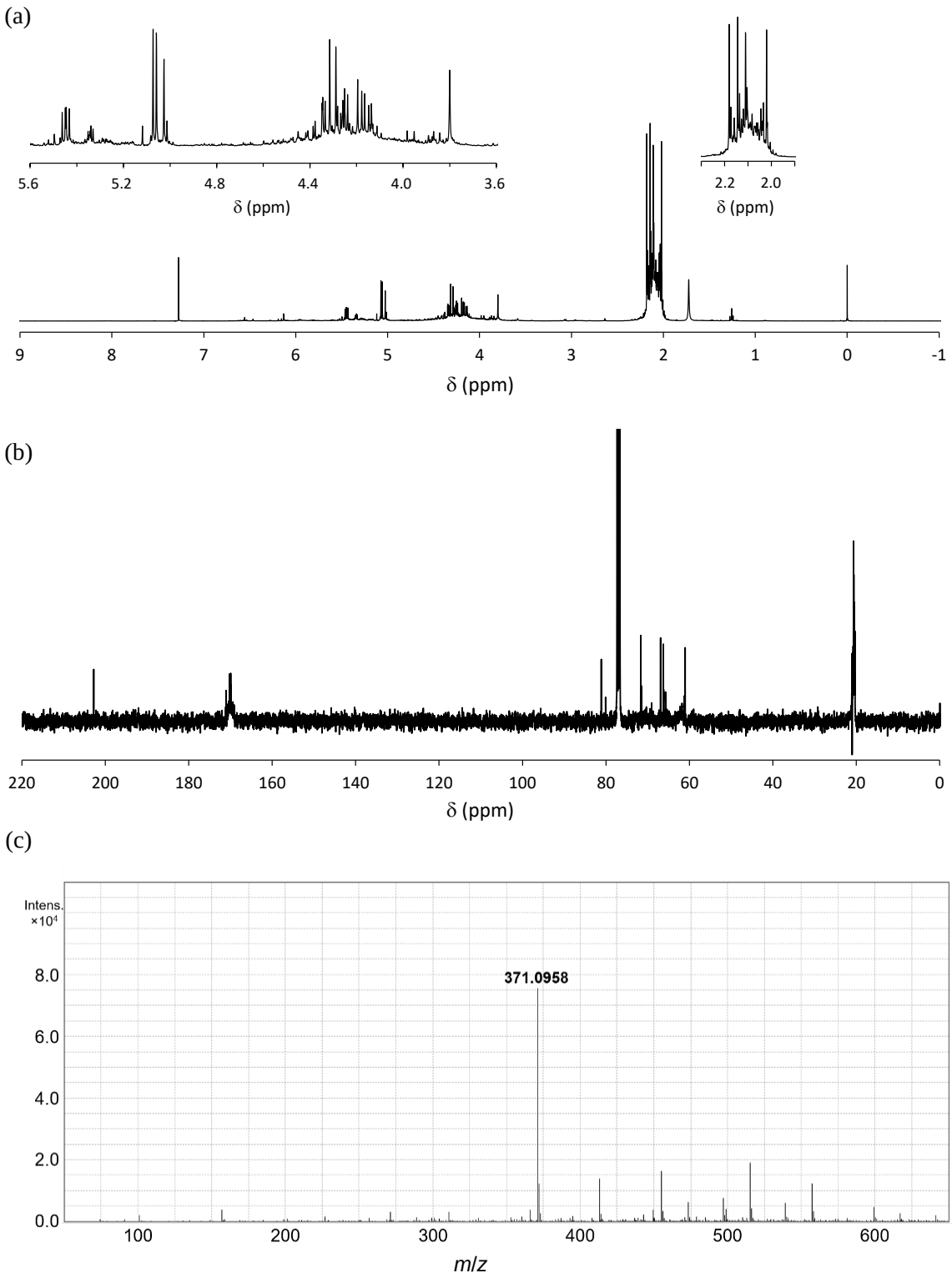

Fig. S24 ^{1}H-NMR, ^{13}C-NMR, and ESI-MS spectra of monohydroxy-3-oxohexanetetrayl tetraacetate. (a) ^{1}H-NMR spectrum. (Insets) Expanded images of spectrum. (b) ^{13}C-NMR spectrum. (c) ESI-MS spectrum.

Table S1. Reaction rates estimated using the Eyring equation for reactions at 353 K (80 °C). A first-order reaction was assumed.

	$\Delta G^{\ddagger}$ (kcal mol^{-1})	k (s^{-1})	$t_{1/2}$
Retro-aldol reaction (Na_2WO_4)	24.19	7.93×10^{-3}	8.74×10^{1} s
Aldol reaction (NaOH)	6.14	1.16×10^{9}	5.96×10^{-10} s
Cannizzaro reaction (NaOH)	11.85	3.39×10^{5}	2.04×10^{-6} s
Aldol reaction (Na_2WO_4)	18.65	2.12×10^{1}	3.28×10^{-2} s
Cannizzaro reaction (Na_2WO_4)	38.66	8.81×10^{-12}	2.49×10^{3} yr

The reaction rate constant k was calculated using the following equation (1):

$$k = \frac{k_B T}{h} exp\left(-\frac{\Delta G^{\ddagger}}{RT}\right) \qquad (1)$$

Assuming that all reactions were first order, the half-life ($t_{1/2}$) was calculated using the following equation (2):

$$t_{1/2} = \frac{ln(2)}{k} \qquad (2)$$

Table S2. Conversion ratio of HCHO to various products formed in the formose reaction with Na_2WO_4 as a catalyst (the reaction condition was same as Fig. 5a, b).

Classification	Name	Conversion ratio of HCHO / %
C2–C4 sugar	Glycolaldehyde (**C2a**)	2.5
	Glyceraldehyde (**C3a**)	1.0
	Dihydroxyacetone (**C3k**)	3.4
	Erythrose (**C4a**)	8.1
	Erythrulose (**C4k**)	10.8
	Total	25.9
C5 sugar	Ribose	1.0
	Arabinose	1.5
	1,3,4-trihydroxy-3-(hydroxymethyl)butan-2-one (A) 1,3,4,5-tetrahydroxypentan-2-one (C5 ketose, **C5k**; B)[*1]	5.3
	Other C5 sugars (determined by phenol-sulfuric acid method)	2.0
	Total	9.8
C6 sugar	Tagatose	0.8
	Sorbose	2.9
	Fructose	2.0
	Mannose	2.0
	Glucose	0.1
	Galactose	0.1
	1,2,4,5,6-pentahydroxyhexan-3-one (3-hexulose, C and D)[*2]	4.5
	Other C6 sugars (determined by phenol-sulfuric acid method)	13.3
	Total	25.5
Sugar alcohol[*3]	C2–OH	0.2
	C3–OH	0.5
	C4–OH	2.7
	C5–OH	1.7
	C6–OH	5.4
	Total	10.5
Organic acid	Formic acid	2.2
Total		73.9

*1 The concentration was estimated from the correlation between the consumption of **C4k** and the peak areas of A and B in the aldol reaction of **C4k** with HCHO (Fig. 4c).
*2 The concentration was estimated from the correlation between the consumption of **C4k** and the peak areas of C and D in the aldol reaction of **C4k** with **C2a** (Fig. 4d).
*3 The concentration of sugar alcohol produced by the crossed Cannizzaro reaction was estimated from the formic acid concentration quantified by HPLC (Fig. 5b).

Table S3. Energies of HOMO of bases and anti-bonding orbital σ* of acids.

Base	Energy of HOMO (eV)	Acid (H-A)	Energy of anti-bonding orbital σ* of H-A (eV)
OH^-	−5.491	Hydrated HCHO ($HO-CH_2-OH$)	−0.236
WO_4^{2-}	−6.350	β-OH in **C4a**	−0.325
		α-hydrogen in **C2a**	−1.429

References

1. M. Dubois, K. A. Gilles, J. K. Hamilton, P. A. Rebers and F. Smith, Colorimetric Method for Determination of Sugars and Related Substances, *Anal. Chem.*, 1956, **28**, 350-356.
2. S. Kato, M. Takashino, K. Igarashi and W. Kitagawa, Isolation and Genomic Characterization of a Proteobacterial Methanotroph Requiring Lanthanides, *Microbes Environ.*, 2020, **35**.
3. S. Quaiyum, K. Igarashi, T. Narihiro and S. Kato, Microbial Community Analysis of Anaerobic Enrichment Cultures Supplemented with Bacterial Peptidoglycan as the Sole Substrate, *Microbes Environ.*, 2020, **35**.
4. M. J. T. Frisch, G. W.; Schlegel, H. B.; Scuseria, G. E.; Robb, M. A.; Cheeseman, J. R.; Scalmani, G.; Barone, V.; Mennucci, B.; Petersson, G. A.; et al., Gaussian 09, Revision E.01, 2009.
5. A. D. Becke, Density‐functional thermochemistry. III. The role of exact exchange, *J. Chem. Phys.*, 1993, **98**, 5648-5652.
6. A. D. Becke, Density-functional exchange-energy approximation with correct asymptotic behavior, *Phys. Rev. A*, 1988, **38**, 3098-3100.
7. C. Lee, W. Yang and R. G. Parr, Development of the Colle-Salvetti correlation-energy formula into a functional of the electron density, *Phys. Rev. B*, 1988, **37**, 785-789.
8. S. H. Vosko, L. Wilk and M. Nusair, Accurate spin-dependent electron liquid correlation energies for local spin density calculations: a critical analysis, *Can. J. Phys.*, 1980, **58**, 1200-1211.
9. W. J. Hehre, R. Ditchfield and J. A. Pople, Self—Consistent Molecular Orbital Methods. XII. Further Extensions of Gaussian—Type Basis Sets for Use in Molecular Orbital Studies of Organic Molecules, *J. Chem. Phys.*, 1972, **56**, 2257-2261.
10. P. C. Hariharan and J. A. Pople, The influence of polarization functions on molecular orbital hydrogenation energies, *Theor. Chim. Acta*, 1973, **28**, 213-222.
11. M. M. Francl, W. J. Pietro, W. J. Hehre, J. S. Binkley, M. S. Gordon, D. J. DeFrees and J. A. Pople, Self‐consistent molecular orbital methods. XXIII. A polarization‐type basis set for second‐row elements, *J. Chem. Phys.*, 1982, **77**, 3654-3665.
12. M. J. Frisch, J. A. Pople and J. S. Binkley, Self‐consistent molecular orbital methods 25. Supplementary functions for Gaussian basis sets, *J. Chem. Phys.*, 1984, **80**, 3265-3269.
13. T. Clark, J. Chandrasekhar, G. W. Spitznagel and P. V. Schleyer, Efficient Diffuse Function-Augmented Basis Sets for Anion Calculations. Iii. The 3-21+G Basis Set for First-Row Elements, Li-F, *J. Comput. Chem.*, 1983, **4**, 294-301.
14. P. J. Hay and W. R. Wadt, Ab initio effective core potentials for molecular calculations. Potentials for K to Au including the outermost core orbitals, *J. Chem. Phys.*, 1985, **82**, 299-310.
15. P. J. Hay and W. R. Wadt, Ab initio effective core potentials for molecular calculations. Potentials for the transition metal atoms Sc to Hg, *J. Chem. Phys.*, 1985, **82**, 270-283.
16. W. R. Wadt and P. J. Hay, Ab initio effective core potentials for molecular calculations. Potentials for main group elements Na to Bi, *J. Chem. Phys.*, 1985, **82**, 284-298.
17. K. Fukui, The Path of Chemical-Reactions - the Irc Approach, *Acc. Chem. Res.*, 1981, **14**, 363-368.
18. H. P. Hratchian and H. B. Schlegel, Using Hessian updating to increase the efficiency of a Hessian based predictor-corrector reaction path following method, *J. Chem. Theory Comput.*, 2005, **1**, 61-69.
19. S. Grimme, J. Antony, S. Ehrlich and H. Krieg, A consistent and accurate ab initio parametrization of density functional dispersion correction (DFT-D) for the 94 elements H-Pu, *J. Chem. Phys.*, 2010, **132**, 154104.
20. J. Tomasi, B. Mennucci and R. Cammi, Quantum mechanical continuum solvation models, *Chem. Rev.*, 2005, **105**, 2999-3093.
21. A. E. Reed, L. A. Curtiss and F. Weinhold, Intermolecular Interactions from a Natural Bond Orbital, Donor-Acceptor Viewpoint, *Chem. Rev.*, 1988, **88**, 899-926.
22. J.-R. Aviles-Moreno and T. R. Huet, Sugars in the gas phase: The conformational properties of erythrose, threose, and erythrulose characterized by quantum chemistry calculations, *J. Mol. Struct. THEOCHEM*, 2008, **858**, 113-119.